Elimination of Current Blocking in Ternary InAlAs-InGaAs-InAlAs Double Heterojunction Bipolar Transistors

M. Mohiuddin, *Member, IEEE*, Tauseef Tauqeer, J. Sexton, R. Knight, and M. Missous, *Senior Member, IEEE*

***Abstract*—Molecular beam epitaxy-grown wafers are used to fabricate all ternary $In_{0.52}Al_{0.48}As$-$In_{0.53}Ga_{0.47}As$-$In_{0.52}Al_{0.48}As$ double heterojunction bipolar transistors (DHBTs) with knee voltages of less than 1 V, showing no current blocking characteristic even at current densities of 200 kA/cm^2. A set of wafers with a judicious combination of doping interface dipoles and composite collector designs were grown, and devices with a wide range of emitter areas from 20×20 down to 1×5 μm^2 were fabricated to investigate the effects of the different epitaxial and geometrical design tradeoffs that culminated in an optimum design that is able to achieve high breakdown and high current gain without introducing current blocking. Despite the use of a heavy dipole doping of 4×10^{18} cm^{-3}, a breakdown voltage BV_{CEO} of 5.8 V at 0.2 kA/cm^2 is achieved at room temperature. We believe this to be the first demonstration of an all-ternary large band gap InAlAs–InGaAs–InAlAs DHBTs with no current blocking up to a high current density of 200 kA/cm^2. These new DHBTs that use only ternary alloys may lead to simplified device growth and fabrication options and give deeper understanding of the design tradeoffs in these structures.**

***Index Terms*—Current blocking, doping interface dipole (DID), double heterojunction bipolar transistor (DHBT), molecular beam epitaxy (MBE).**

I. Introduction

THE SUPERIOR performance of $In_{0.52}Al_{0.48}As$-$In_{0.53}Ga_{0.47}As$ single heterojunction bipolar transistors (SHBTs) for low-power and high-speed communication applications at 40 GHz and above is well established [1]. However, high-power microwave or precision mixed-signal applications require large breakdown and/or higher early voltage. These characteristics are achieved by using double heterojunction bipolar transistor (DHBT) implementations where a large band gap material is used in the collector region to reduce the deleterious effect of impact ionization in the otherwise low band gap material ($In_{0.53}Ga_{0.47}As$) in the collector region of SHBT. This, however, introduces a large energy barrier at the base–collector (B–C) interface that impedes carrier flow across the junction, appreciably reducing the current gain. This reduction is usually referred to as current blocking [2], and it is directly proportional to the conduction band discontinuity ΔE_c at the B–C heterojunction. Current blocking in DHBTs with $In_{0.52}Al_{0.48}As$ collectors is much more pronounced as compared with those with InP collectors because of the unfavorable band alignment [3] at the $In_{0.52}Al_{0.48}As$-$In_{0.53}Ga_{0.47}As$ heterojunction. Many researchers [4]–[6] investigated current blocking in $In_{0.52}Al_{0.48}As$ or quaternary InAlGaAs collector-based DHBTs and used either super lattice and/or grading at the heterojunctions as a partial solution to the problem. In most cases, current blocking can only be removed when quaternary alloys are used in the collector since these tend to have lower ΔE_c, but this is usually at the expense of a much reduced breakdown value. McAlister *et al.* [7] and others [8]–[11] used a combination of dipole doping [12] and setback layer in DHBTs of different materials to reduce current blocking. However, to the best of the authors' knowledge, appreciable or complete elimination of current blocking in $In_{0.52}Al_{0.48}As$-$In_{0.53}Ga_{0.47}As$-$In_{0.52}Al_{0.48}As$ DHBTs up to current densities of 200 kA/cm^2 using only ternary alloys have not been reported to date. This has been achieved with an optimized combination of setback layers and doping interface dipole (DID) and without resorting to more complex growth techniques like interface grading and Coherent Heterointerfaces for Reflection and Penetration superlattice.

Manuscript received April 25, 2010; accepted August 27, 2010. Date of publication October 4, 2010; date of current version November 19, 2010. This work is supported in part by European Community and in part by the Science and Technology Facilities Council as part of the Square Kilometre Array Design Studies program and the Electro Magnetic Remote Sensing Defence Technology Centre on high speed heterojunction bipolar transistors. The review of this paper was arranged by Editor S. Bandyopadhyay.

M. Mohiuddin was with the School of Electrical and Electronic Engineering, The University of Manchester, M13 9PL Manchester, U.K. He is now with the Karachi Institute of Economics and Technology, Karachi 75190, Pakistan.

T. Tauqeer was with the School of Electrical and Electronic Engineering, The University of Manchester, M13 9PL Manchester, U.K. He is now with the School of Electrical Engineering and Computer Science, National University of Sciences and Technology, Islamabad 54000, Pakistan.

J. Sexton, R. Knight, and M. Missous are with the School of Electrical and Electronic Engineering, The University of Manchester, M13 9PL Manchester, U.K. (e-mail: m.missous@manchester.ac.uk).

Color versions of one or more of the figures in this paper are available online at http://ieeexplore.ieee.org.

Digital Object Identifier 10.1109/TED.2010.2074203

II. Epitaxial Structure Growth and Device Fabrication

A. Wafer Growth and Epitaxial Layers

Wafers were grown on a Riber V100+ solid source molecular beam epitaxy on $\langle 100 \rangle$-oriented semiinsulating Fe-doped InP

TABLE I
EPITAXIAL STRUCTURE OF THE
$In_{0.52}Al_{0.48}As$-$In_{0.53}Ga_{0.47}As$-$In_{0.52}Al_{0.48}As$ DHBTs

Layer	Material	Thickness(Å)	Doping (cm^{-3})
Cap1	$In_{0.53}Ga_{0.47}As$	800	$2x10^{19}$ (n)
Cap2	$In_{0.52}Al_{0.48}As$	800	$2x10^{19}$ (n)
Emitter	$In_{0.52}Al_{0.48}As$	500	$5x10^{17}$ (n)
Spacer	$In_{0.53}Ga_{0.47}As$	100	nid
Base	$In_{0.53}Ga_{0.47}As$	650	$2x10^{19}$ (p)
Setback	$In_{0.53}Ga_{0.47}As$	500 (Sample 1&2) 750 (Sample 3)	$1x10^{16}$ (n)
n spike	$In_{0.52}Al_{0.48}As$	50 (Sample 1)	$2x10^{18}$ (n)—Sample 1
p-n dipole doping	$In_{0.53}Ga_{0.47}As$ - $In_{0.52}Al_{0.48}As$	2 x 100	$3x10^{18}$ (pn)—Sample 2 $4x10^{18}$ (pn)—Sample 3
Collector	$In_{0.52}Al_{0.48}As$	2000	$1x10^{16}$ (n)—Sample 1 $5x10^{16}$(n)—Sample 2&3
Collector 2	$In_{0.52}Al_{0.48}As$	500	$1x10^{19}$ (n)
Sub-collector	$In_{0.52}Ga_{0.47}As$	3500	$1x10^{19}$ (n)
Buffer	$In_{0.52}Al_{0.48}As$	300	nid
Substrate	InP		Semi-insulating

nid = no intentional doping

substrates. Si and Be are used as n- and p-type dopants, respectively. The entire epitaxial structure comprises $In_{0.52}Al_{0.48}As$ and $In_{0.53}Ga_{0.47}As$ lattice-matched layers to the InP substrate; no quaternary alloys are used in the structure.

Ten wafers with distinct combination of setback layer thickness, dipole, and collector doping were grown and both large- and small-area devices were fabricated and measured; however, in this paper, only three of these samples are discussed to illustrate the design tradeoffs for current blocking elimination. Common and distinct epilayers of these samples are given in Table I. A salient feature of all these epitaxial structures is the insertion of an $In_{0.53}Ga_{0.47}As$ setback layer between the base and the collector. First, an $In_{0.52}Al_{0.48}As$ n-spike with doping 2×10^{18} cm^{-3} is introduced in the collector layer (sample 1). Later, this n-spike is replaced by a dipole layer comprising a p-type layer of $In_{0.53}Ga_{0.47}As$ on the $In_{0.53}Ga_{0.47}As$ setback layer side and another n-type layer of $In_{0.52}Al_{0.48}As$ on the $In_{0.52}Al_{0.48}As$ collector side of the B–C junction with the doping of 3×10^{18} (sample 2) and 4×10^{18} cm^{-3} (sample 3). The base–emitter (B–E) heterojunction is abrupt and includes an $In_{0.53}Ga_{0.47}As$ spacer layer of 100-Å thickness. Table I gives details of the epitaxial structures.

B. Device Fabrication

Large-emitter-area devices of 20×20 μm^2 and small-geometry RF devices of emitter areas 1×5 and 1×10 μm^2 were fabricated using a triple-mesa wet-etching process. Epitaxial layers were first etched using a nonselective orthophosphoric-based etchant $H_3PO_4 : H_20_2 : H_20$ (3 : 1 : 50). This was followed by a short selective etch of HCl : H_20 (3 : 1) to expose the InGaAs base and subcollector layers. Nonalloyed Ti/Au contacts to the emitter, base, and subcollector layers were then thermally evaporated to complete the devices.

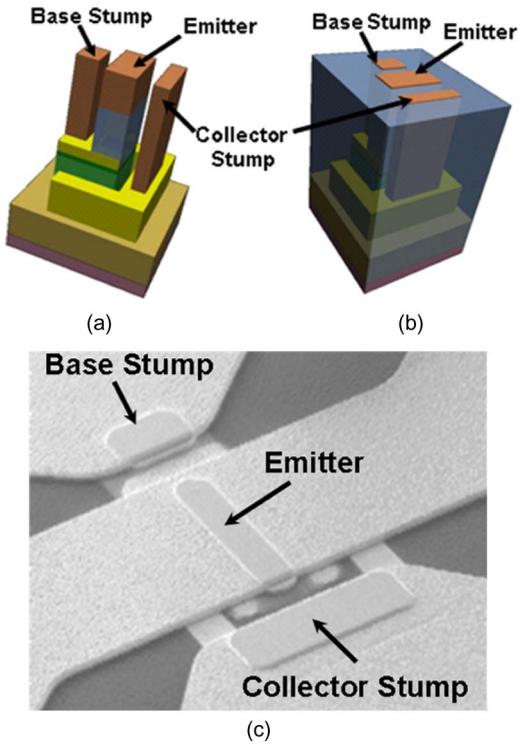

Fig. 1. (a) Planarized contacts. (b) Exposed contacts through BCB. (c) SEM image of a sample-3 device with an emitter area of 1×5 μm^2.

To increase the yield of the process, stumps were introduced to make planarized ohmic contacts, as shown in Fig. 1(a) and (b). In addition, shown in Fig. 1(c) is the scanning electron microscope (SEM) image of a finished sample-3 device of emitter dimensions (1×5) μm^2.

III. DYNAMICS OF CURRENT BLOCKING EFFECT

The SILVACO ATLAS 2-D physical simulator [13] is used to calculate the equilibrium band diagrams (see Figs. 2–5) for a typical DHBT epitaxial structure to illustrate the effect of setback layers and dipole dopings. All the included band diagram models are basic models that are given under thermodynamic equilibrium to illustrate the role of the spacer, setback, and dipole layers and are part of the ongoing work using the SILVACO ATLAS 2-D simulations with the ultimate aim of accurate predictions of the dc and RF performances.

Beryllium out diffusion [14] into the emitter–base spacer layer is simulated by assuming this layer to be doped at 10% of the base doping level. The abrupt base–emitter junction is used to facilitate hot-electron launching as it causes a higher ratio of perpendicular to parallel electron velocity [15], which also helps in the effective reduction of the current blocking. Arguments both in favor [2], [4] and against [16] the abrupt B–E junction for $In_{0.53}Ga_{0.47}As$-InP HBTs are prevalent in the literature where smaller $V_{CE(offset)}$ is traded with simpler growth technique and hot-electron launching.

The large band gap discontinuity of the B–C junction can be partially reduced by the introduction of a setback layer. Fig. 2 illustrates the effect of introducing a setback layer of 500 Å on

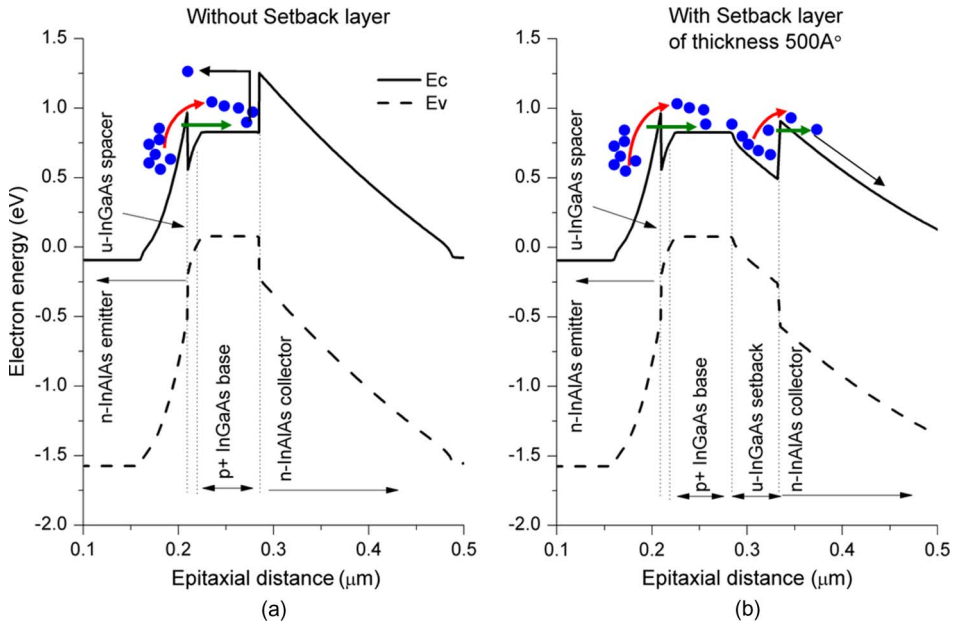

Fig. 2. Simulated band diagrams of the DHBT (a) without and (b) with the setback layer of 500 Å.

the band diagram. The amount of band bending on both sides of a heterojunction is in inverse proportion to their doping [15] such that the lightly doped side of the junction bends more than the heavily doped side. Fig. 2(a) shows the band diagram of the InAlAs–InGaAs DHBT without the setback layer. Since the interface is between a very heavily doped base and a lightly doped collector region, it results in a large B–C junction spike, as shown in Fig. 2(a). However, the insertion of a setback layer increases band bending on the $In_{0.53}Ga_{0.47}As$ side of the B–C heterointerface, forcing the band spike down and resulting in the start of a carrier flow across the B–C junction, as shown in Fig. 2(b).

Despite appreciable reduction in the band spike that is relative to the conduction band edge at the base, the barrier for electrons still remains at the B–C heterojunction. The setback layer actually transforms a step barrier into a wide triangular quantum well [17]–[20], as can be seen in Fig. 2(b). Although due to the band slope in the setback layer and the resultant electric field, the electrons attain energy as they go downhill, and the transport across the B–C heterojunction improves; however, the barrier is not completely eliminated.

Since the use of composite collector reduces and transforms the step barrier into a triangular quantum well, under forward bias conditions, electrons exiting the base experience the supportive electric field and are swept across. However, due to the presence of the triangular well, most of the electrons cannot cross the B–C heterojunction and, rather, get trapped in the well and start piling up, as shown in Fig. 2(b). This electron pileup starts to screen out the field across the B–C junction, and due to this effective reduction in electric field, electrons acquire less energy from the B–C reverse-bias voltage. At this stage, there are very few electrons that make it to the collector, and the predominant transport mechanism across the B–C junction is tunneling. As the base collector bias is increased further, this leads to increased tunneling across the B–C heterointerface,

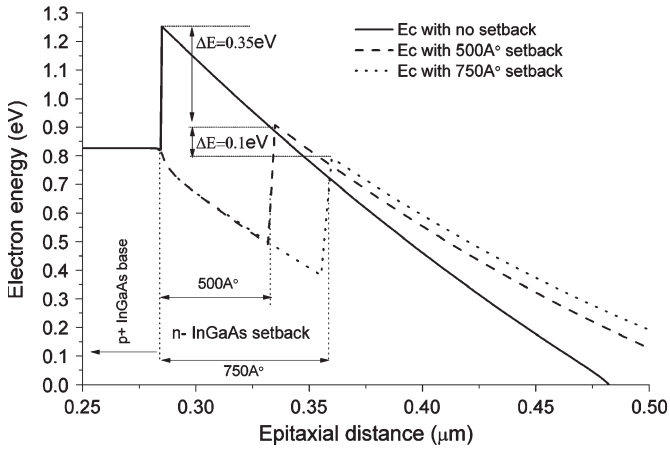

Fig. 3. Effect of the setback layer thickness on the band diagram.

which impacts current flow across the B–C heterointerface in two ways.

1) Increased tunneling directly raises the current flow across the B–C junction, leading to larger collector current.
2) As the electrons escape the quantum well, their screening effect on the original electric field (due to B–C reverse bias) is also reduced. With the reappearance of the larger electric field across the B–C junction, electrons attain higher energy as they go downhill across the junction, leading to enhanced thermionic emission across the B–C energy barrier [17], [20].

This positive feedback causes a switching of transport mechanism from predominantly tunneling to thermionic emission across the BC heterointerface and gives rise to precipitous increase in the collector current; this phenomenon is called switching effect in DHBTs [2], [7], [17], [20].

To further observe the effect of increasing the setback layer thickness, SILVACO simulations were performed, and the

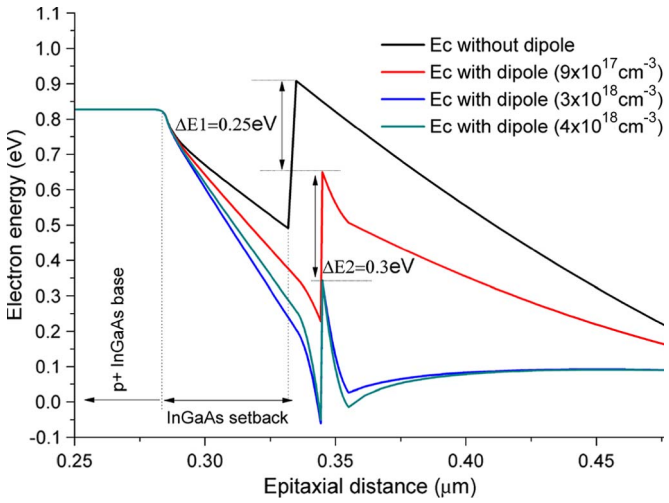

Fig. 4. Effect of the DID on the band diagram.

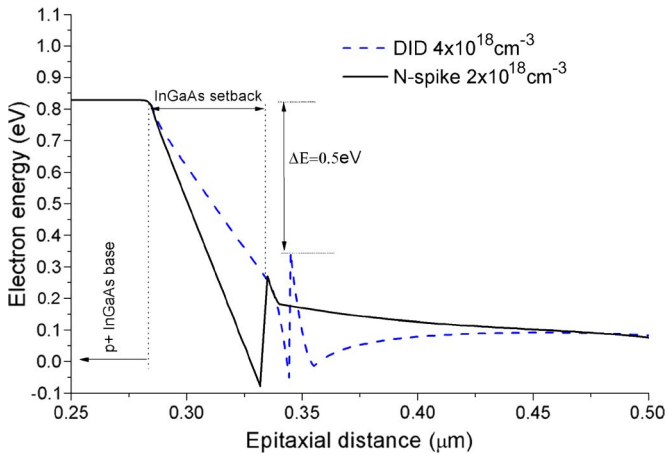

Fig. 5. Comparison of the energy band models of samples 1 and 3.

setback layer was increased from 500 to 750 Å; the results are shown in Fig. 3, which clearly indicates that larger thickness lowers the band spike. However, the amount of lowering is about 33% as compared with the 50% increase in the thickness of the setback layer; furthermore, it is extremely important to note that the setback layer is of a smaller band gap material (InGaAs), and its larger value invariable reduces the breakdown voltage, which nullifies the basic advantage of high breakdown of the DHBTs. From these considerations, a thickness of 750 Å was considered to be the maximum limit for the setback layer for these epitaxial structures.

In agreement with earlier studies [2], [19], in order to improve carrier transport across the B–C junction, a suitable electric field was introduced to counteract the screening effect of the electron pileup. This electric field, in addition to reducing the screening effect of electron pileup, also improves carrier transport in a subtle way, as explained next.

The wider triangular quantum that is well formed at the B–C heterojunction, as shown in Fig. 2(b) and in Fig. 3, has shallow subband energy levels, as estimated by the following relationship for infinite triangular wells [21]:

$$E_i = \left(\frac{\hbar^2}{2m^*}\right)^{1/3} \left(\frac{3\pi}{2} q\xi_S\right)^{2/3} \left(i - \frac{1}{4}\right)^{2/3}. \qquad (1)$$

Where E_i is the energy level of index i, $\hbar$ and ξ_S are reduced the Planck's constant and the effective electric field, respectively, m^* is the electron effective mass, and q is electronic charge. Even with this approximate model, it is clear that the energy barrier at the B–C interface can be further reduced by increasing the effective electric field as it raises the energy levels of the subbands for the electrons in the quantum well by reducing its thickness. Fig. 4 simulates the impact of introducing a DID as its doping is increased from 9×10^{17} to 4×10^{18} cm^{-3}. In these epitaxial structures, the DID is essentially composed of two oppositely doped layers of 100-Å thickness straddling the B–C heterojunction. Fig. 4 shows that with the introduction of the DID, not only does the band spike go further down, which facilitates the carrier conduction, but also, both the thickness of the quantum well on the base side of the junction and the thickness of the barrier on the collector side of the junction are reduced. It is also important to observe that the incremental effect of the dipole doping reduces as the doping level is progressively increased.

The reduction in the thickness of the quantum well raises the subband energy levels, which increases the probability of thermionic emission across the junction, and the reduction of barrier facilitates the tunneling across the junction. To highlight the difference between the effect of the n-spike and the DID on the energy bands of the structure, a one-to-one comparison of band models of samples 1 and 3 are shown in Fig. 5. Clearly, the DID results in the symmetrical band bending on either sides of the junction resulting in both the narrower quantum well on the left-hand side of the interface and narrower barrier on the right-hand side of the interface, whereas the n-spike only reduces the thickness of the energy barrier and does not influence the quantum well thickness. Overall, the dipole dramatically improves the device performance by increasing the carrier transport manifolds across the B–C junction as is observed in the measured data that are discussed next.

IV. Results and Discussions

Fig. 6 shows the I–V curves of sample 1, which elucidates the switching effect as discussed earlier very well. The large knee voltage that is coupled with a precipitous rise in the current as the reverse bias is increased clearly highlights the presence of both the current blocking and the switching effect. The abrupt rise in the output current is proportional to the base current because the larger the base current, the higher the pileup of carriers at the B–C interface and, hence, the larger is the change in the value of the collector current at the instant of switching from predominantly tunneling to thermionic emission.

However, to see the incremental impact of introducing a suitable electric field, first, an n+ spike in the collector layer was introduced. This did not result in acceptable device performance as is evidenced by the I–V curves of sample 1 that includes an n+ spike that is doped at 2×10^{18} cm^{-3} and still has a large current blocking resulting in an impractically high $V_{\mathrm{CE(offset)}}$ of 4 V and a knee voltage of 5.6 V. These

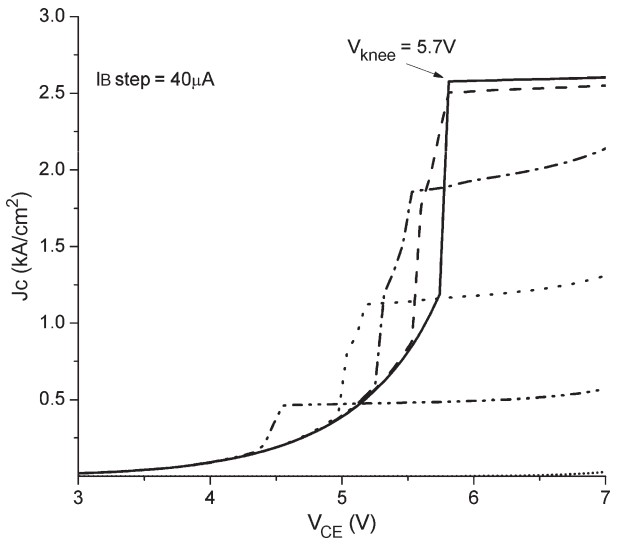

Fig. 6. DC I–V curves of sample 1 showing excessive current blocking.

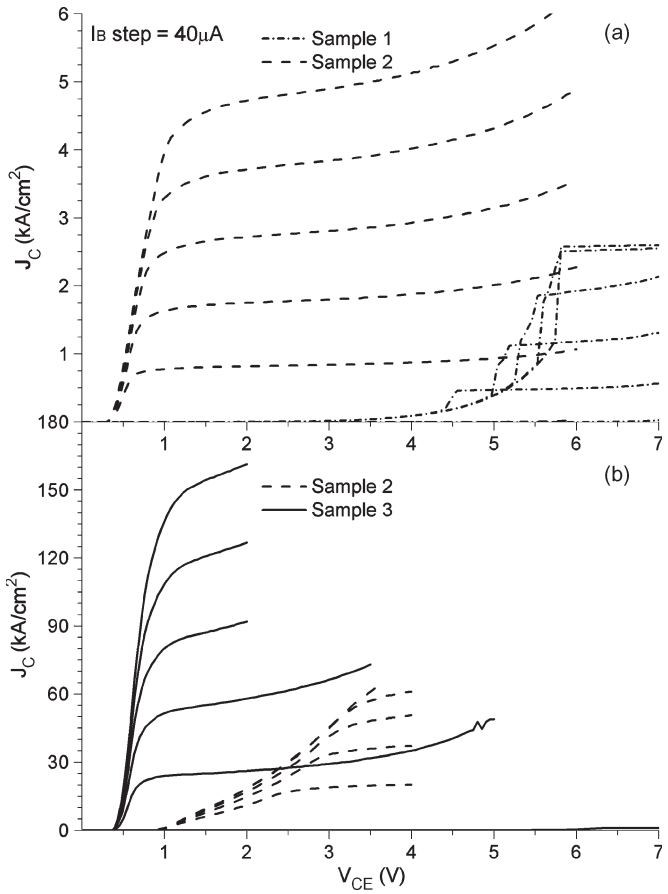

Fig. 7. DC I–V curves of (a) samples 1 and 2 at current density < 10 kA/cm^2 (b) samples 2 and 3 at current density up to 150 kA/cm^2.

values correspond well with earlier reported results [2]. To fully eliminate current blocking, the n-spike was replaced by a dipole that is doped at 3×10^{18} cm^{-3} across the B–C junction. This resulted in much improved I–V curves with lower knee voltage, indicating less carrier accumulation at the B–C spike even at a little larger values of J_C [5], as shown in Fig. 7(a) (sample 2). However, as the current density was increased toward the

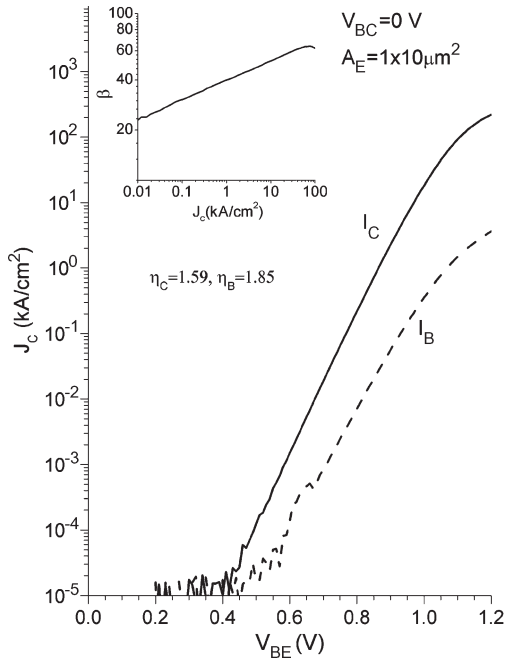

Fig. 8. Gummel plot and current gain versus current density curve of sample 3.

value of 100 kA/cm^2 (which is the minimal current density to achieve high f_T), a very large knee voltage of larger than 3 V is observed for a current density of about 50 kA/cm^2, as shown in Fig. 7(b) for sample 2. To get an improved device performance at higher current densities, a better tradeoff between the elimination of current blocking and breakdown voltage was achieved by increasing the setback layer to 750 Å with an increased dipole doping of 4×10^{18} cm^{-3}. In agreement with the simulations, as shown in Figs. 3 and 4, respectively, it resulted in complete elimination of the current blocking as is evidenced by the comparison of I–V curves of samples 2 and 3 that are shown in Fig. 7(b). Despite the availability of empirical models (Agilent HBT) that have been developed by the authors for circuit simulations that are based on these devices, only the measured data are shown because the empirical models are based on the measured data and, hence, do not independently reflect the underlying physics of the device. For example, it does not account for the breakdown mechanism due to impact ionization.

The Gummel plot and current gain versus the current density curve of sample 3 are shown in Fig. 8, which shows a variation of current gain from 25 to ∼60 as the current density is increased from 0.01 to more than 100 kA/cm^2. These results are superior to the earlier reported results for abrupt B–E, all-ternary InAlAs emitter DHBTs [22] and comparable with InAlAs emitter DHBTs with quaternary alloys [5], [15] but with the added advantage of much higher breakdown voltages. Reasonable gain over a wide range of current density is desirable as it results in increased linearity of the amplifiers over a wider power range and also helps in low-power analog circuit design.

The collector current ideality factor η_C of 1.59 is slightly higher compared with earlier reported results [4], [15]; a higher value of η_C in the range 1.4–1.5 is routinely observed in abrupt B–E junction InAlAs HBTs primarily due

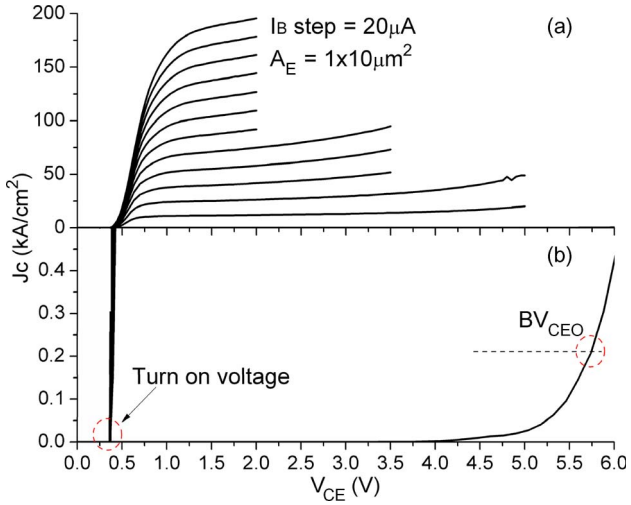

Fig. 9. Sample 3 (a) I–V curves (b) Turn-on and breakdown characteristics.

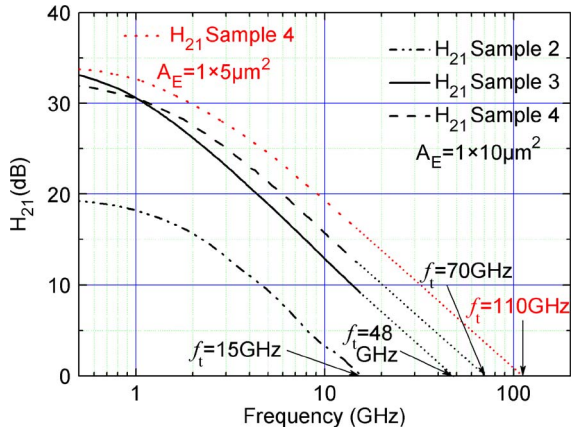

Fig. 10. RF measurements (cutoff frequencies) of the samples.

to the large conduction band discontinuity of about 0.5 eV, which promotes tunneling as the predominant transport mechanism. As mentioned earlier, despite the B–E spacer layer, Beryllium out diffusion occurs, which causes the reappearance of the band spike resulting in larger value of collector current ideality.

However, the ideality factor of the base current is determined by the weighted average of all its components. Briefly, there are three components of base current that is relevant for this discussion: $I_{\rm NBR}$ (neutral base recombination current), $I_{\rm BSCR}$ (space-charge base recombination current), and $I_{\rm BIB}$ (back-injection base current) as surface recombination is negligible in the InAlAs/InGaAs material system. Out of these components of base current, only $I_{\rm BSCR}$ has an ideality factor of 2; the other components show characteristic diffusive behavior and have an ideality factor of 1 [23]. Hence, a larger base current ideality factor is attributed to higher space-charge recombination current in comparison with the other components of base current, which could be due to the presence of lattice imperfections and dopant sites. Despite this rather large values of the ideality factors, sample 3 has excellent common–emitter I–V curves and breakdown characteristics, as shown in Fig. 9. In order to avoid interface grading, an abrupt B–E interface is used. The abrupt B–E heterointerface is known to cause higher offset voltage due to the large conduction band discontinuity of the InAlAs/InGaAs heterointerface. The ratio of the emitter-to-collector areas did not make an appreciable effect on $V_{\rm CE(offset)}$ as its value remained between 0.3 and 0.35V when the emitter area was reduced from 100×100 to 1×5 μm^2.

To the best of the authors' knowledge, which is supported by extensive literature search [4], [5], [7], [22], [24], this is the first demonstration of the complete elimination of current blocking in all-ternary InAlAs–InGaAs–InAlAs DHBTs even at a current density of 200 kA/cm^2 and with a knee voltage that is less than 1 V and a breakdown $\rm BV_{CEO}$ of 5.8 that is measured at 0.2 kA/cm^2. Current densities in the range of 100–200 kA/cm^2 are invariably required to achieve higher cutoff frequency for high-speed digital or microwave applications. However, the optimum current density for the highest f_T depends on many factors, including the material system and geometrical and epitaxial design. For example, Griffith *et al.* [25] showed that with a 0.6-μm emitter width, the optimum current density is about 600–800 kA/cm^2 for their transferred substrate process devices; however, more recently, Driad *et al.* [26], using more relaxed geometry of 1×4 μm^2 and normal substrate techniques, showed that the optimum current density was in the range 300–400 kA/cm^2. Similarly, Freeman *et al.* [27] showed that its value varied from 100 to 200 kA/cm^2 as the device emitter area was reduced from 1 to 0.18 μm^2. For our devices, we found this optimum value to remain in the range of 100 to 200 kA/cm^2.

Normally, at higher current densities, both self-heating and impact ionization effects occur; at lower values of output voltage, the resultant common–emitter I–V curves may or may not explicitly show one or the other effect, despite its presence, due to the predominance of the other. However, as the voltage increases, then, in the case of HBTs and in the presence of excessive self-heating, the I–V curves show a distinct negative slope resulting in the decrease in the collector current. At even higher voltages due to excessive impact ionization effect, it ultimately leads to an exponential rise in the collector current. On the contrary, in the case of negligible self-heating effect, a negative slope region does not occur. We observed self-heating effects in only a few of the small emitter area $(1 \times 10$ μm$^2)$ devices, and most of the devices that are measured did not show self-heating characteristics.

Fig. 10 shows the RF performance of the samples. Since sample 2 was not an optimized structure, it shows a very low value of f_T of 15 GHz. In the fabrication of sample-3 RF devices, air-bridges have been used for the base contacts to reduce the B–C capacitance; however, during the later stages of processing, the etching profile of the benzocyclobutene (BCB) resist was not well controlled and did not undergo enough lateral etching, which resulted in larger values than that of the normal values of the of B–C capacitance, limiting the cutoff frequency f_T to about 50 GHz. The graph also shows the RF performance of our latest run of another sample, i.e., sample 4, with epitaxial structure that is similar to that of sample 3 but with a thinner base of 450 Å. The improvement has mainly been in the parasitic B–C capacitance that was reduced by a factor of approximately 3 as compared with sample 3, further

confirming the less-than-optimum processing to be the primary cause for the inferior RF performance of sample 3.

Some electronic warfare and wireless local area network applications [28] of these devices require a dc current gain of 50, with an average cutoff and maximum oscillation frequency of about 100 GHz; furthermore, the breakdown voltage $BV_{CEO} > 5$ V is required, and $V_{CE(offset)} \leq 0.2$ V is desirable. Sample 3 meets all the required dc specifications, and with the aforementioned process improvements, such as the case of Sample 4, it will also meet the RF performance specifications.

The SHBTs with similar epitaxial design, except for the essential difference of the collector material, were fabricated, and their maximum current density was found to be comparable with that of the DHBT in sample 3. Current densities that are higher than 200 kA/cm^2 caused a larger knee voltage in the SHBTs, also further confirming the upper bound of the current density to be primarily limited by the Kirk effect.

V. Conclusion

Elimination of current blocking at the B–C interface has been reported for the first time in an all-ternary $In_{0.52}Al_{0.48}As$-$In_{0.53}Ga_{0.47}As$-$In_{0.52}Al_{0.48}As$ DHBT up to a current density of 200 kA/cm^2. This has been accomplished with the correct combination of spacer thickness and dipole doping, without sacrificing the crucial high breakdown characteristics. The elimination of the current blocking is leading to ongoing high frequency investigations where both maximum oscillation frequency and cutoff frequency that is greater than 100 GHz (on 1×5 μm^2 devices) have so far been obtained.

The higher breakdown voltages that are available in $In_{0.52}Al_{0.48}As$ should permit the implementation of higher power devices.

Acknowledgment

M. Mohiuddin and T. Tauqeer would like to thank the Higher Education Commission, Islamabad, Pakistan, and the National University of Science and Technology, Islamabad, Pakistan, for their support.

References

[1] M. Sokolich, C. H. Fields, S. Thomas, B. Q. Shi, Y. K. Boegeman, M. Montes, R. Martinez, A. R. Kramer, and M. Madhav, "A low-power 72.8-GHz static frequency divider in AlInAs/InGaAs HBT technology," *IEEE J. Solid-State Circuits*, vol. 36, no. 9, pp. 1328–1334, Sep. 2001.

[2] W. R. McKinnon, R. Driad, S. P. McAlister, A. Renaud, and Z. R. Wasilewski, "Temperature independent current blocking due to hot electrons in InAlAs/InGaAs double heterojunction bipolar transistors with composite collectors," *J. Vac. Sci. Technol. A, Vac. Surf. Films*, vol. 16, no. 2, pp. 846–849, Mar. 1998.

[3] I. Vurgaftman, J. R. Meyer, and L. R. Ram-Mohan, "Band parameters for III-V compound semiconductors and their alloys," *J. Appl. Phys.*, vol. 89, no. 11, pp. 5815–5875, Jun. 2001.

[4] C. H. Huang, T. L. Lee, and H. H. Lin, "Relation between the collector current and the 2-dimensional electron-gas stored in the base–collector heterojunction notch of InAlAs/InGaAs/InAlGaAs DHBTs," *Solid State Electron.*, vol. 38, no. 10, pp. 1765–1770, Oct. 1995.

[5] T. Iwai, H. Shigematsu, H. Yamada, T. Tomioka, K. Joshin, and T. Fujii, "1.5 V low-voltage microwave power performance of InAlAs/InGaAs double heterojunction bipolar transistors," *Jpn. J. Appl. Phys. 1, Regul. Papers Short Notes Rev. Papers*, vol. 36, no. 2, pp. 648–651, Jan. 1997.

[6] C. Nguyen, T. Y. Liu, M. Chen, H. C. Sun, and D. Rensch, "AlInAs/GaInAs/InP double heterojunction bipolar transistor with a novel base–collector design for power applications," *IEEE Electron Device Lett.*, vol. 17, no. 3, pp. 133–135, Mar. 1996.

[7] S. P. McAlister, W. R. McKinnon, R. Driad, and A. P. Renaud, "Use of dipole doping to suppress switching in indium phosphide double heterojunction bipolar transistors," *J. Appl. Phys.*, vol. 82, no. 10, pp. 5231–5234, Nov. 1997.

[8] S. Yamahata, K. Kurishima, H. Ito, and Y. Matsuoka, "Over-220-GHz-fT-and-fmax InP/InGaAs double-heterojunction bipolar transistors with a new hexagonal-shaped emitter," in *Proc. 17th Annu. GaAs IC Symp. Tech. Dig.*, 1995, pp. 163–166.

[9] W. Liu and D. S. Pan, "Proposed collector design of double heterojunction bipolar transistors for power applications," *IEEE Electron Device Lett.*, vol. 16, no. 7, pp. 309–311, Jul. 1995.

[10] T. Ishibashi and Y. Yamauchi, "A possible near-ballistic collection in an AlGaAs/GaAs HBT with a modified collector structure," *IEEE Trans. Electron Devices*, vol. 35, no. 4, pp. 401–404, Apr. 1988.

[11] Q. J. Hartmann, M. T. Fresina, D. A. Ahmari, and G. E. Stillman, "Effect of collector design on the d.c. characteristics of $In_{0.49}Ga_{0.51}P$/GaAs heterojunction bipolar transistors," *Solid State Electron.*, vol. 38, no. 12, pp. 2017–2021, Dec. 1995.

[12] F. Capasso, A. Y. Cho, K. Mohammed, and P. W. Foy, "Doping interface dipoles—Tunable heterojunction barrier heights and band-edge discontinuities by molecular-beam epitaxy," *Appl. Phys. Lett.*, vol. 46, no. 7, pp. 664–666, Apr. 1985.

[13] *ATLAS Manual*, SILVACO Int., Santa Clara, CA, 2005.

[14] S. R. Bahl, N. Moll, V. M. Robbins, H. C. Kuo, B. G. Moser, and G. E. Stillman, "Be diffusion in InGaAs/InP heterojunction bipolar transistors," *IEEE Electron Device Lett.*, vol. 21, no. 7, pp. 332–334, Jul. 2000.

[15] B. Jalali, "Current transport in an abrupt HBT," in *InP HBTs—Growth, Processing, and Applications*, B. Jalali and S. J. Pearton, Eds. Norwood, MA: Artech House, 1994.

[16] J. A. Baquedano, A. F. J. Levi, and B. Jalali, "Comparison of graded and abrupt junction $In_{0.53}Ga_{0.47}As$ heterojunction bipolar-transistors," *Appl. Phys. Lett.*, vol. 64, no. 1, pp. 67–69, Jan. 1994.

[17] S. P. McAlister, W. R. McKinnon, Z. Abid, and E. E. Guzzo, "Hysteresis in the switching of hot-electrons in InP/InGaAs double-heterojunction bipolar-transistors," *J. Appl. Phys.*, vol. 76, no. 4, pp. 2559–2561, Aug. 1994.

[18] R. L. Liboff, *Introductory Quantum Mechanics,* 4th ed. San Francisco, CA: Addison-Wesley, 2003.

[19] W. R. McKinnon, "One-flux analysis of current blocking in double-heterostructure bipolar transistors with composite collectors," *J. Appl. Phys.*, vol. 79, no. 5, pp. 2762–2770, Mar. 1996.

[20] D. Ritter, R. A. Hamm, A. Feygenson, H. Temkin, M. B. Panish, and S. Chandrasekhar, "Bistable hot-electron transport in InP/GaInAs composite collector heterojunction bipolar-transistors," *Appl. Phys. Lett.*, vol. 61, no. 1, pp. 70–72, Jul. 1992.

[21] P. Harrison, *Quantum Wells, Wires and Dots: Theoretical and Computational Physics of Semiconductor Nanostructures,* 3rd ed. Chichester, U.K.: Wiley, 2009.

[22] B. Jalali, R. N. Nottenburg, Y. K. Chen, A. F. J. Levi, D. Sivco, A. Y. Cho, and D. A. Humphrey, "Near-ideal lateral scaling in abrupt $Al_{0.48}In_{0.52}As/In_{0.53}Ga_{0.47}As$ heterostructure bipolar-transistors prepared by molecular-beam epitaxy," *Appl. Phys. Lett.*, vol. 54, no. 23, pp. 2333–2335, Jun. 1989.

[23] W. Liu, *Handbook of III-V Heterojunction Bipolar Transistors*. New York: Wiley, 1998.

[24] R. Driad, W. R. McKinnon, S. P. McAlister, A. Renaud, and Z. R. Wasilewski, "Temperature independent current blocking in InAlAs/InGaAs double heterojunction bipolar transistors with composite collectors," in *Proc. IEEE/Cornell Conf. Adv. Concepts High Speed Semicond. Devices Circuits*, 1997, pp. 123–131.

[25] Z. Griffith, M. Dahlstrom, M. J. W. Rodwell, X. M. Fang, D. Lubyshev, Y. Wu, J. M. Fastenau, and W. K. Liu, "InGaAs-InP DHBTs for increased digital IC bandwidth having a 391-GHz f(T) and 505-GHz fmax," *IEEE Electron Device Lett.*, vol. 26, no. 1, pp. 11–13, Jan. 2005.

[26] R. Driad, R. E. Makon, V. Hurm, K. Schneider, F. Benkhelifa, R. Losch, and J. Rosenzweig, "InP DHBT-based ICs for 100 Gbit/s data transmission," in *Proc. 20th Int. Conf. Indium Phosphide Related Mater.*, Versailles, France, 2008, pp. 247–250.

[27] G. Freeman, B. Jagannathan, S. J. Jeng, J. S. Rieh, A. D. Stricker, D. C. Ahlgren, and S. Subbanna, "Transistor design and application considerations for >200-GHz SiGe HBTs," *IEEE Trans. Electron Devices*, vol. 50, no. 3, pp. 645–655, Mar. 2003.
[28] J. D. Cressler, "Emerging application opportunities for SiGe technology," in *Proc. IEEE Custom Integr. Circuits Conf.*, San Jose, CA, 2008, pp. 57–64.

M. Mohiuddin (M'92) received the B.E. degree in electrical engineering from NED University of Engineering and Technology, Karachi, Pakistan in 1992, the M.S. degree in electrical engineering from the University of Nebraska, Lincoln, in 1996, and the Ph.D. degree in electrical and electronic engineering from The University of Manchester, Manchester, U.K., in 2010.

After working for Caterpillar Inc., Pakistan, for about a year, he proceeded to the United States for graduate studies. During his M.S. degree, he worked on optical characterization applying Raman spectroscopy and ellipsometry techniques on heavily doped bulk InGaAs and GaAs/AlGaAs multiple quantum wells. After finishing his M.S. degree in 1996, he remained associated with Electrical and Computer Engineering departments of various engineering institutions in Pakistan as a full-time faculty member. He has recently joined Karachi Institute of Economics and Technology, Karachi, Pakistan, as an Associate Professor. His current research interests entail physical and empirical device modeling and RF measurements of InP double-heterojunction bipolar transistors and high-electron mobility transistors for high-speed low-power digital applications.

Tauseef Tauqeer received the M.S. degree in communication engineering and the Ph.D. degree in microelectronics and nanostructures from The University of Manchester, Manchester, U.K., in 2006 and 2009, respectively.

He is currently appointed as an Assistant Professor with the School of Electrical Engineering and Computer Sciences, National University of Science and Technology, Islamabad, Pakistan. He has extensively worked on the physical device modelling and simulation of III–V-based materials. He is also actively involved in the design and fabrication of InP-based low-power gigahertz-class analog-to-digital converters for the international Square Kilometre Array radio telescope.

J. Sexton, photograph and biography not available at the time of publication.

R. Knight, photograph and biography not available at the time of publication.

M. Missous (M'95–SM'05) leads the Microelectronic and Nanostructure Group, The University of Manchester, Manchester, U.K. He has a proven track record of technology transfer, and a strong feature of his work is the close industrial involvement he maintains with the leading players in the microwave field. Examples of these include the design and molecular beam epitaxial growth of graded-gap Gunn diodes for e2v Ltd. for use in Intelligent Cruise Control systems in cars at 77 GHz, with fully working devices fitted in BMW and Audi cars. He is developing technologies for the international Square Kilometre Array radio telescope, which involves the design and fabrication of super low noise receivers and super fast analog-to-digital converters at $\sim$4 GHz using advanced InP technology.